# Morphological responses and sediment processes following a typhoon-induced dam failure, Dahan River, Taiwan

**Desiree Tullos[1]\* and Hsiao-Wen Wang[2]**
[1] Department of Biological and Ecological Engineering, 116 Gilmore Hall, Corvallis Oregon, 97331, USA
[2] Department of Hydraulic and Ocean Engineering, National Cheng Kung University, Taiwan

\*Correspondence to: D. Tullos, Department of Biological and Ecological Engineering, 116 Gilmore Hall, Corvallis Oregon, 97331, USA. E-mail: desiree.
tullos@oregonstate.edu

*ESPL*
Earth Surface Processes and Landforms

ABSTRACT: The rates and styles of channel adjustments following an abrupt and voluminous sediment pulse are investigated in the context of site and valley characteristics and time-varying sediment transport regimes. Approximately $10.5 \times 10^6 \, m^3$ of stored gravel and sand was exposed when Barlin Dam failed during Typhoon WeiPa in 2007. The dam was located on the Dahan River, Taiwan, a system characterized by steep river gradients, typhoon- and monsoon-driven hydrology, high, episodic sediment supply, and highly variable hydraulic conditions. Topography, bulk sediment samples, aerial photos, and simulated hydraulic conditions are analyzed to investigate temporal and spatial patterns in morphology and likely sediment transport regimes. Results document the rapid response of the reservoir and downstream channel, which occurred primarily through incision and adjustment of channel gradient. Hydraulic simulations illustrate how the dominant sediment transport regime likely varies between study periods with sediment yield and caliber and with the frequency and duration of high flows. Collectively, results indicate that information on variability in sediment transport regime, valley configuration, and distance from the dam is needed to explain the rate and pattern of morphological changes across study periods. Copyright © 2013 John Wiley & Sons, Ltd.

KEYWORDS: sediment pulse; dam removal; channel recovery; Taiwan; Barlin Dam; sediment transport regime

## Introduction

Channel response to sediment pulses are qualitatively predictable, with conceptual models offering important guidance for managing habitat and infrastructure impacts with deliberate pulse releases (Bartley and Rutherfurd, 2005; Hoffman and Gabet, 2007). However, quantitative projection of channel response is a challenging problem due to the complex linkages between hydraulic and sediment processes at basin and local scales. To better understand rates and patterns of channel recovery (sensu Wolman and Gerson, 1978) following a sediment pulse, a growing number of field studies, laboratory experiments, and numerical models have been conducted (see Lisle, 2008 for review; Sklar *et al.*, 2009; Venditti *et al.*, 2010; Humphries *et al.*, 2012). These studies have identified factors that contribute to variability in the rates and patterns in channel response to a sediment pulse. The list of driving factors includes characteristics of: (a) the channel, such as channel gradient, width, depth, bank saturation vegetation, exposed bedrock, and large wood and other roughness features of the channel (Doyle *et al.*, 2002; Madej, 2001; Simon *et al.*, 2000); (b) the stored and ambient bed sediment, including its volume, grain size, consolidation, stratification, and cohesion (Madej and Ozaki, 1996; Lisle *et al.*, 2001; Pizzuto, 2002; Doyle *et al.*, 2002, 2003; Sawaske and Freyberg, 2012);

and (c) the flow regime following the sediment release, particularly the frequency, intensity, and timing of high flows (Wohl and Cenderelli, 2000; Doyle *et al.*, 2002; Hassan and Zimmermann, 2012; Major *et al.*, 2012; but also see Sawaske and Freyberg, 2012).

While studies regarding sediment pulses have been conducted under a range of hydrogeographic conditions (Doyle *et al.*, 2003; Kasai *et al.*, 2004; Gran and Montgomery, 2005; Major *et al.*, 2012), there remains a need to evaluate the existing empirical knowledge and conceptual models for sites outside the range of conditions for which current understanding was developed. Quantitative and mechanistic understanding of channel responses to sediment pulses will be more complete with the inclusion of cases from areas of the world with strongly seasonal hydrology, high discharge and sediment yields, steep to moderate gradients, and event-driven sediment delivery and transport. Furthermore, efforts are still needed to better understand how local and basin-scale factors contribute to the hydraulic conditions and sediment transport regimes that govern rates and patterns in processing a sediment pulse. Linking channel morphology and sediment transport processes may clarify how governing factors vary within and across basins and regions.

In this study, we document rates and styles of channel adjustments following an abrupt and voluminous sediment pulse in a
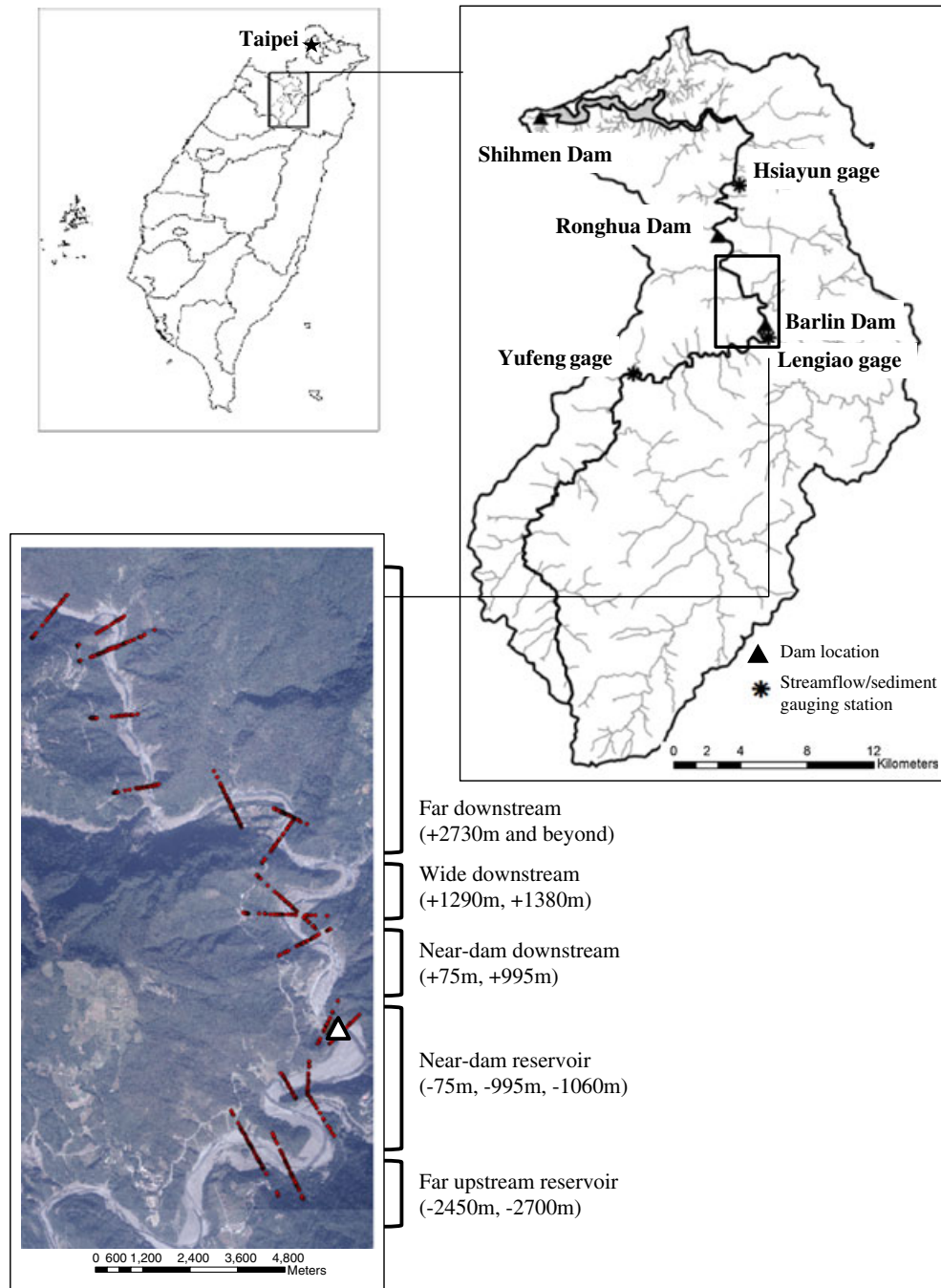
**Figure 1.** Site map of study area, dam and gauging station locations, and study subreaches. Red dots represent locations of analyzed survey points along pre-failure cross-sections. The white triangle is the site of the former dam.

system characterized by highly-variable sediment and hydraulic conditions, we analyze site and valley characteristics and to investigate factors governing the rates and character of observed channel adjustments over time. Our analysis is conducted on the Dahan River, Taiwan, along a reach upstream and downstream of the Barlin Dam site, which failed during Typhoon WeiPa in September 2007. For both the reservoir and downstream channel, we ask: (a) across periods of different sediment transport regimes, what are the rates and spatial patterns of channel adjustment?; and (b) over the study periods prior to and following dam failure, what were the likely sediment transport regimes generated by the basin-scale sediment and hydrologic inputs? The study adds new, though imperfect, documentation of rapid channel response to a large pulse of sediment released in a system of highly variable transport capacity

and loads, with interpretation of the channel processes that likely drove the observed responses.

## Study Area

The Dahan River, a major tributary to the Tamsui River, drains a geologically-active 1163 km$^2$ basin in the northern Central Range of Taiwan (Figure 1). The basin is characterized by steep hillslopes, exceeding 55% in over two-thirds of the drainage basin, fractured bedrock, intense monsoonal precipitation, and frequent landsliding. Annual hydrology in the basin undergoes a monsoon season (May–June) and a typhoon season (July–October), with consistently low baseflow occurring in the period between (November–April).

Barlin Dam, constructed on the Dahan River in 1977, was a 38-m-high concrete gravity dam with rotary-arm gates. In combination with Ronghua Dam 11.6 km downstream (Figure 1) and over 100 smaller structures, Barlin Dam was constructed with the primary purpose of retaining sediment. The suite of dams are part of a basin-wide strategy to maintain the capacity of a large water supply (municipal, industrial and irrigation), hydropower, and flood management reservoir (Shihmen) downstream (Figure 1).

Barlin Dam's initial storage capacity of $10.5 \times 10^6$ m$^3$ was filled with sediment by 2003, 26 years after it was completed. A 'defense dam,' constructed immediately downstream of Barlin Dam for energy dissipation, was critically damaged by undercutting (TWRA, 2007) during Typhoon Aere in 2004 and failed completely in 2006 (Figure 2). Incision then propagated upstream to the base of Barlin Dam, which failed during Typhoon WeiPa in September 2007, a roughly 1-year return event with an estimated peak discharge of 225 m$^3$/s (Figure 3).

The morphology of the channel around Barlin Dam is structured by the basin hydrology and local valley configuration. In our study section, the Dahan River drains a 765 km$^2$ forested landscape. Half of the contributing area drains from Sankuan Creek, which enters the east side of the reservoir approximately 1500 m upstream of the former dam site. The river pattern is valley-forced meandering, with resistant bedrock lining the valley walls. Unvegetated point bars, established along the inside of meander bends, are inundated in most years. Across the study reach, the channel gradient is 1% and sinuosity is 1.7. Prior to dam failure in 2006, the active channel width varied between 55 m and 315 m across the study section and the bed substrate was comprised of non-cohesive coarse sand to very fine gravel. Despite the forested nature of the catchment, in-channel wood was not observed during site visits in 2009 and 2012 and does not appear to be an important component of channel roughness or structure.

Although the volume of sediment stored behind Barlin Dam was large, the Dahan River has a high capacity for transporting the stored sediment. We estimate that the dam stored approximately 20 years of average annual sediment loads. This estimate is based on a mass ratio of stored sediment ($17.8 \times 10^6$ tonnes) to average annual transported total load ($0.837 \times 10^6$ tonnes). The mass of stored sediment is estimated by assuming a bulk density of 1.7 tonnes/m$^3$ and a reservoir full of sediment ($10.5 \times 10^6$ m$^3$). The total load transported annually is estimated based on combining: (1) long-term (1957–2002) suspended sediment rating curves (TWRA, 2006) at the Yufeng gauging station (Figure 1), with (2) the observation that suspended load comprises approximately 70% of the total load in Taiwan's rivers (Dadson et al., 2003). We thus estimate the average suspended load and bed load for the Yufeng station to be $0.583 \times 10^6$ tonnes per year and $0.251 \times 10^6$ tonnes per year, respectively. These large sediment loads are matched by monsoon- and typhoon-driven high flows, which generate high sediment transport capacities in some years. The long-term average annual runoff volume for the Dahan River at the former dam site is $64.8 \times 10^8$ m$^3$, though this discharge is delivered to the channel in a few, intense runoff events. Thus, the erosional efficiency, calculated as the ratio of volume of sediment stored to volume of annual streamflow, is 0.0016 for the study reach, a value that is high relative to other rivers globally (Sawaske and Freyberg, 2012).

However, the transport capacity varies considerably along the study reach with valley and channel configuration. We thus have delineated sub-reaches (Figure 1) within the reservoir and downstream channels based on variability in active channel width (Figure 4(c)) and gradient (Table I). While sediment in the reservoir extended approximately 4000 m upstream of the former dam, our reservoir study reach extends only 2700 m due to limits of the topographic surveys. The first three cross-sections (–75 m, –910 m, –1060 m) upstream of the dam, henceforth referred to as the 'near-dam reservoir' reach, are characterized by a relatively narrow valley width and



| October 2002 | September 2005 |
| August 2006 | November 2007 |

**Figure 2.** Sequence of photographs looking upstream at Barlin Dam and its failure in 2007. Note the exposure and extent of the reservoir sediment in 2005. The defense dam, which was critically damaged during Typhoon Aere in 2004, completely failed in 2006. (Photos courtesy of Taiwan Water Resources Agency, used with permission.)
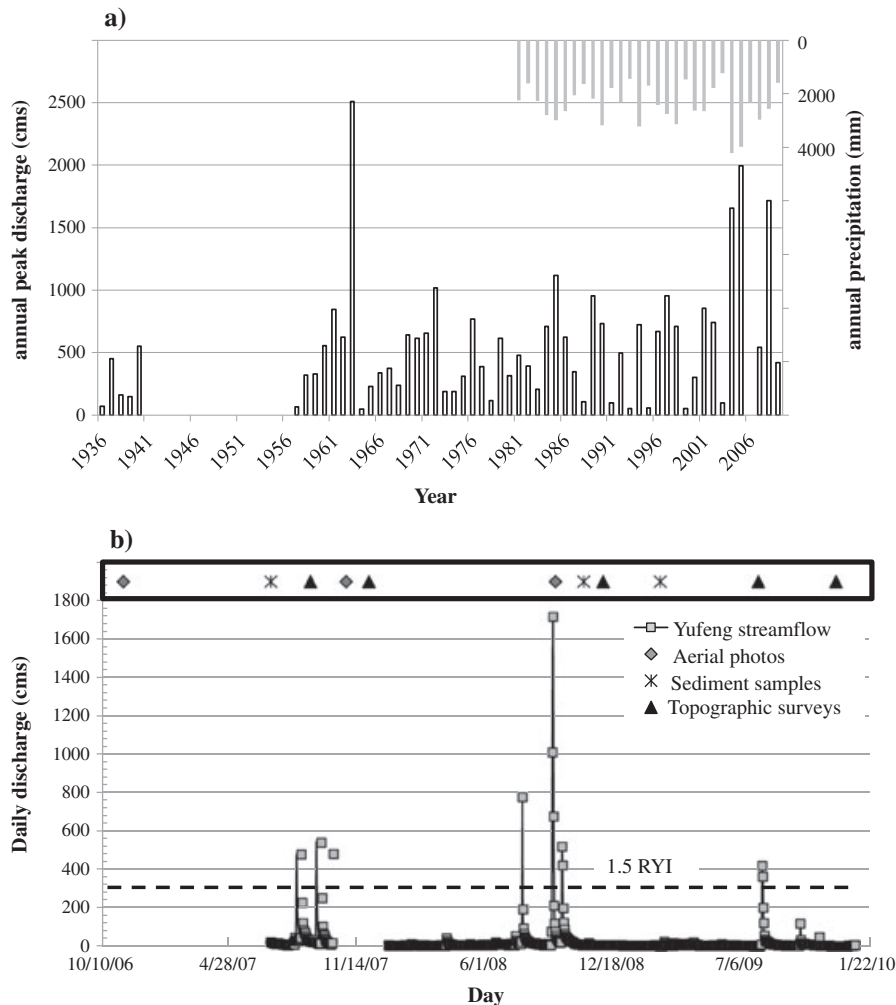
a)



b)



**Figure 3.** (a) Historical annual peak discharge at the Yufeng station and precipitation at the Lengiao station (cf. Figure 1), and (b) daily discharge at Yufeng station from 2007 to 2010 and dates of sampling events. No discharge data were available for 1941–1956 or 2006. Dashed line in Figure 3(b) represents value of 1.5 RYI (309 m$^3$/s).

generally single-thread channel (Figure 4(c)). For the cross-sections ,–2450 m, –2700 m, upstream of the near-dam reservoir reach (henceforth referred to as 'far-upstream reservoir' reach), the valley widens appreciably and the river transitions to a multi-thread channel (Figure 4(c)). The entire downstream study reach extends 6800 m below Barlin Dam, to the reservoir formed by Ronghua Dam (Figure 1). We subdivide the downstream channel into three reaches (Figure 1). The first two cross-sections (+75 m, +995 m) downstream of the dam, henceforth referred to as 'near-dam downstream' reach, are located within a narrow, single-thread channel (Figure 4(c)). Below this reach, over a length of approximately 1700 m, the valley widens within the 'wide-downstream reach,' represented by two wide (Figure 4(c)) cross-sections (+1290 m and +1380 m). The third downstream reach, henceforth referred to as 'far downstream reach,' extends approximately 4000 m beyond the wide-downstream reach in a narrow, single-thread channel (Figure 4(c)).

## Methods

We analyze topographic surveys, sediment samples, discharge records, and aerial photos, all acquired from the TWRA as part of their ambient monitoring program. Within this monitoring program, the timing (Figure 3(b)) and extents of surveys varied between years. As a result, more robust techniques for analysis

of channel change (e.g. Wheaton *et al.*, 2010) are not possible with this dataset. To the extent possible, we provide estimates of error (e.g. volumes of eroded/deposited material), and attempt to acknowledge the limitations of the datasets and approaches applied herein. Results and interpretations are supported by field visits in 2009 and 2012 during which locations of exposed bedrock, terraces, and active landslides were mapped along the study reach, and qualitative field interpretations of active geomorphic processes were made.

## Topography

Topographic surveys were conducted prior to and following the failure of Barlin Dam. The timing (Figure 3(b)) of topographic surveys generally align with the start and end of the typhoon season and are the basis for our definition of study periods (Table II). The pre-failure survey, conducted in September 2007, included cross-sections surveyed at approximately 200 m spacing. In subsequent surveys (Figure 3(b)), topography was mapped with the intent of generating contour maps, with emphasis on defining depositional features and the main channel at baseflow. This contour-based approach resulted in an irregular sampling scheme with typical point densities of 1 point per 290 m$^2$. The extents of the surveys also vary between years. For example, the first survey following the dam failure, conducted in December 2007, is the shortest in longitudinal
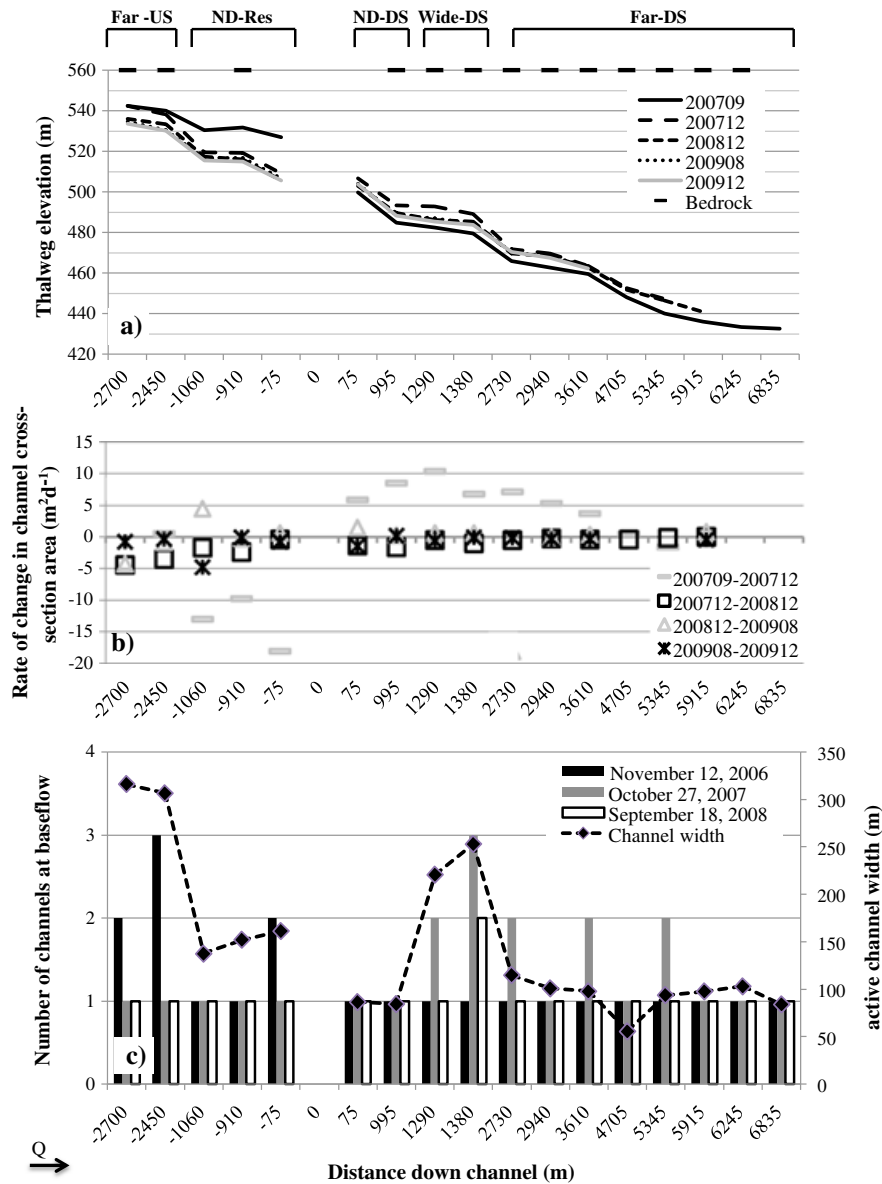
**Figure 4.** (a) Thalweg elevations and presence of exposed bedrock (elevation not represented); (b) rate of change in cross-sectional area. Missing data (e.g. below 5400 m downstream in December 2007) are not represented in the figure. (c) The number of channels at baseflow for each aerial photo and the active channel width based on the 2006 aerial photo. Flow (Q) direction is to the right of the page.

extent, including only 5400 m of the channel downstream from the dam. Subsequent surveys extend farther downstream but irregularly exclude portions of the channel.

All surveys were conducted by total station and only in wadeable areas. Based on pre-failure aerial photos and field visits in 2009 and 2012, this wadeable survey approach precluded surveying the thalweg in a few areas. However, based on visual inspection of the survey points, the maximum gap in survey points for the deepest parts of the channel appears

to be consistently small (<2 m) across the entire study area. Unfortunately, the lack of thalweg elevation observations introduces unknown error into the channel surveys and estimates of volume changes.

Though the contour-based surveys conducted after dam failure more evenly sampled the entire channel, because pre-failure topographic surveys were based on cross-sections, we performed our comparisons at the pre-failure cross-section locations. We derived elevations for the post-failure surveys at

**Table I.** Channel gradient by reaches and study period. Cross-section locations within each reach are in parentheses.

| Study period | Far-upstream reservoir (−2450 m, −2700 m) | Near-dam reservoir −1060 m) | Near-dam downstream (+75 m, +995 m) | Wide-downstream (+1290 m, +1380 m) | Far downstream (+2730 m and beyond) |
|---|---|---|---|---|---|
| September 2007 | 0.009 | 0.005 | 0.016 | 0.014 | 0.009 |
| December 2007 | 0.010 | 0.012 | 0.015 | 0.011 | 0.011 |
| December 2008 | 0.017 | 0.012 | 0.015 | 0.011 | 0.010 |
| August 2009 | 0.017 | 0.010 | 0.017 | 0.011 | 0.009 |
| December 2009 | 0.013 | 0.010 | 0.017 | 0.012 | 0.010 |

**Table II.** Number of days above 1.5 return year Interval (RYI, 309 m³/s) during each study period.

| Study period | Number of days above 1.5RYI |
|---|---|
| September 2007–December 2007 | 3 |
| December 2007–December 2008 | 6 |
| December 2008–August 2009 | 0 |
| August 2009–December 2009 | 2 |

the locations of the pre-failure cross-sections from Digital Elevation Models (DEMs) created in ArcMap 10. For each DEM, we first generated a Triangulated Irregular Network (TIN) and then linearly interpolated the TIN into a raster. Cross-sectional were then extracted from each post-failure DEM at the locations of the pre-failure cross-sections. Longitudinal profiles were generated by selecting the lowest point in each of the cross-sections as an estimate of the thalweg elevation.

Reach-wide volumes of sediment eroded or deposited are estimated by first calculating the change in cross-sectional area between surveys. We also calculate the area between adjacent points across a cross-section as trapezoids for the two surveyed surfaces. We also calculate volume differences by multiplying the difference in area for the entire cross-section by one half of the distance to adjacent upstream and downstream cross-sections. We calculate rates of change in area at each cross-section as the area of change between survey periods divided by the number of days between survey periods. To distinguish uncertainty from physical change (Fuller *et al.*, 2003; Milan *et al.*, 2007), we calculate a single elevational error for each year based on the average of differences in elevations for repeat points at survey monuments within that survey year. We acknowledge that, without spatially explicit and complete estimates of both random and systematic errors, our uniform application of elevational error may result in conservative estimates of change in areas of low variability and exaggeration of the volumes of erosion and deposition in highly variable areas (Wheaton *et al.*, 2010).

## Sediment samples

Bulk sediment samples of 1 m³ volume were analyzed to characterize longitudinal changes in grain size distributions over time. Sediment samples were collected on exposed gravel bars in the channel once pre-failure and twice post-failure (Figure 3(c)). We note that sample locations and dates do not overlap with surveyed cross-sections. Although the samples were not conducted at the same locations over time, sediment samples were consistently collected using the same procedure over time and samples were always collected on exposed gravel bars such that they are consistent with respect to the type of geomorphic unit sampled. As a result of this sampling program, we present the distribution of grain sizes from the individual samples, but restrict our interpretation to the reach scale. We include results from sediment samples collected approximately 15 km upstream of the former dam site, hereafter referred to as the 'upstream reference' reach, to provide basin-wide context for changes in substrate within the study reach. Box plots are used to characterize the grain size distribution over time. To investigate change in downstream grain sizes relative to the reservoir, we normalize the downstream median (D50) grain sizes by the average reservoir D50, each year.

## Hydrology and hydraulic conditions during annual peak flows

Annual precipitation and peak discharge (Figure 3(a)) illustrate the long-term hydrologic trends. In addition, daily discharge (Figure 3(b)) from the Yufeng gauging station (Figure 1) demonstrate the sequence of flows for each study period. After scaling the discharge from the Yufeng station to the Barlin Dam site by catchment area (335 km²), we estimate the number of days with discharge above the 1.5 return year interval (RYI) at the Barlin Dam site (Table II) as a rough surrogate for channel-forming discharges (Leopold *et al.*, 1964; Williams, 1978). We acknowledge that the 1.5RYI is an imprecise estimate of bed-mobilization even in the systems for which it was evaluated (Williams, 1978). Furthermore, there is likely to be substantial variability in the most effective discharge frequency for event-driven, mountainous rivers (Hassan and Zimmermann, 2012), such as the Dahan River of Taiwan. We thus emphasize that the 1.5RYI is investigated with the intent of distinguishing the relative and general degree of transport potential between the study periods.

An uncalibrated HEC-RAS (USACE, 2011, version 4.1) 1-D, steady flow model is developed to estimate hydraulic conditions for the peak discharge of the downstream reach between each survey period. The goal of this modeling effort is to identify the likely sediment transport processes influencing channel adjustments across the survey periods. The model is used to estimate depth, applied shear stress, Shields number, grain Reynolds number, and grain submergence. These parameters are then related to sediment transport modes and regimes as reported in the literature (Dade and Friend, 1998; Church, 2006). The pre-failure hydraulic conditions are simulated using the pre-failure geometry and pre-typhoon annual peak for the 2007 water year. Hydraulic characteristics for post-failure study periods are simulated using the channel geometry and gradients surveyed at the end of the study period and the peak flow that occurred over the study period that preceded the topographic survey.

## Aerial photos

We analyze aerial photos of the study reach to characterize the planform of the Dahan River during low-flow conditions prior to (2006) and following dam failure (2007, 2008). All photos are of the same scale (1/5000). Flows for the 27 October 2007 and 18 September 2008 photos were both low, 18 m³/s and 14 m³/s, respectively, and representative of the baseflow condition. Unfortunately, no local gages were operating at the time of the 2006 photo. However, the timing of the photo (12 November 2006) after the typhoon season, as well as the photo itself, indicate that discharge on the day of the photo also represents the baseflow condition.

From the three aerial photos, we estimated active channel widths and counted the number of channels observed to be carrying baseflow. While the discharge between the photos is roughly similar, we did not use digitized depositional features to estimate changes in gravel areas or low-flow wetted width. The unquantified exposure errors associated with varying discharge constrain our ability to precisely compare feature boundaries (Walter and Tullos, 2010) and we have no reliable approach for estimating the exposure error. Thus, we present the aerial photo analyses only to support qualitative interpretation of the processes driving channel response. Images from the aerial photos are not presented in the interest of space.

# Results

## Post-failure hydrology

Based exclusively on differences in hydrology across the study periods (Table II, Figure 3(b)), flow records suggest that the most rapid channel change was likely to occur within the first 15 months post-failure. Three days of flows above the 1.5RYI occurred in the 3 months between the pre-failure and post-failure surveys, including Typhoon WeiPa that resulted in the dam failure. The following year experienced 6 days of high discharge. Discharge was low during the subsequent two study periods: no flows greater than 1.5RYI occurred between December 2008 and August 2009, a period that included spring monsoonal rains but not typhoons. Two days of discharge greater than 1.5RYI occurred between August 2009 and December 2009.

## Grain size distribution across the study reach

Owing to inconsistency in the sampling locations longitudinally between years, we interpret the patterns of substrate variability only at reach scale. Furthermore, because no samples were collected in the first 1500 m downstream of the dam site prior to failure, we cannot evaluate changes in bed material size in the near-dam downstream reach.

Prior to dam failure, the bed material was composed mainly of sand and fine gravel (Figure 5(a)) across the entire study site. Grain size did not vary substantially or systematically along the length of the study area, including at the far (~ –15 km) upstream sediment reference sampling locations. The consistent grain size across the study site is likely explained by the fact that the dam had been passing bed load after it filled with sediment in 2003.

By November 2008, the first sediment survey following dam failure, the median and the spread of bed material grain sizes at all locations increased by an order of magnitude (Figure 5(b)) relative to grain sizes observed in the pre-failure survey in July 2007. This increase in bed material size also occurred at the upstream reference locations. These results indicate that a basin-wide coarsening occurred in the year following Typhoon WeiPa. By March 2009 (Figure 5(c)), the median substrate coarsened further in the near-dam reservoir reach, as well as at 4000 m downstream. However, across the study site, the spread of bed substrate distribution was lower in 2009 (Figure 5(c)) than the year following dam failure (Figure 5(b)). These basin-scale trends offer little evidence of impacts of the dam failure on grain size distribution.

The median grain sizes relative to the reservoir substrate sizes offer similarly little evidence of dam failure impacts. Prior to dam failure, median grain sizes in downstream reaches were locally coarser and locally finer than the reservoir D50 (Figure 5 (a)). Relative grain size increases with distance from the dam, though the trend does not appear to be meaningful as the differences in absolute grain sizes are small. In November 2008, the downstream substrate is finer that the reservoir substrate for all sites (Figure 5(b)). Two years after failure, substrate was sampled only in the far downstream reach (Figure 5(c)). The median size of substrate in the far downstream reach is not consistently higher or lower than the reservoir substrate (Figure 5(c)).

Taken together, results offer no conclusive evidence of an effect of dam failure on bed material grain size. It is likely that any effect is obscured by the basin-wide coarsening prior to November 2008 and by limitations of the sediment sampling, including inconsistent sediment sampling locations and the lack of sediment samples in the near-dam reach.
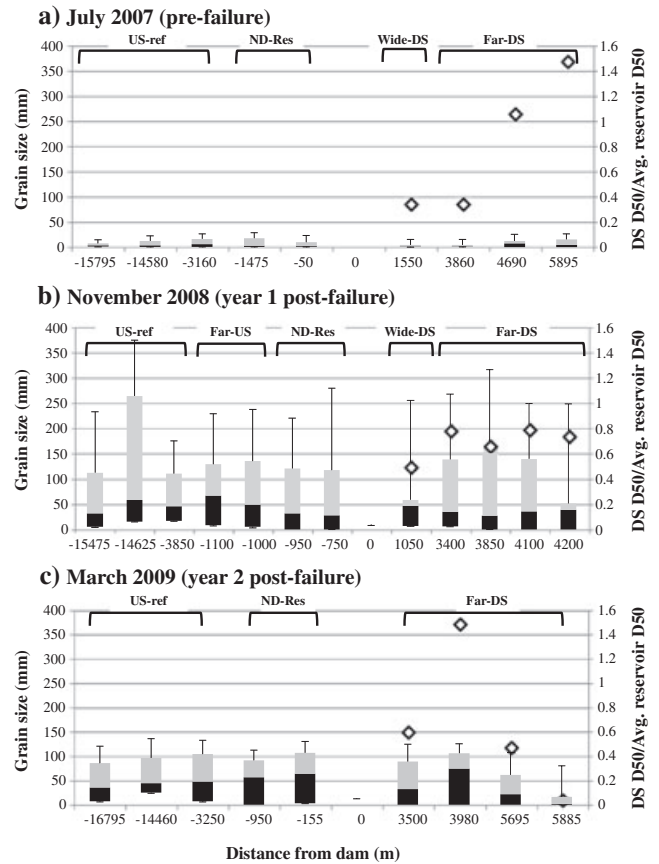


**Figure 5.** Longitudinal variations in grain sizes (a) before failure (July 2007), (b) 14 months after failure (November 2008), and (c) 18 months after failure (March 2009). Each box encompasses the middle 50% of the sample (D25–D75). Whiskers represent D90 and D10 and the D50 is presented as transition between grey and black within the boxes. On the secondary y-axis with diamond symbols, each downstream sediment sample D50 is normalized by the annual average of the reservoir D50. Note the different ranges for the x-axis due to differences in sampling locations between years.

## Rates and patterns of reservoir erosion

Rapid responses of the reservoir to dam failure were restricted to the near-dam reservoir reach. Within the first 3 months following failure, the thalweg (Figure 4(a)) in the near-dam reservoir reach incised up to 18 m. Rates of change in cross-sectional area (Figure 4(b)) were also high for this reach in the first 3 months after dam failure. From September to December 2007, 18 $m^2$ of material eroded per day from the cross-section just upstream of the dam (–75 m). Plots of the cross-sections at –75 m (Figure 6(a)) and –1060 m (Figure 6 (b)) indicate that the erosion in the near-dam reservoir occurred uniformly at a width approximately equivalent to the valley width. Also in the 3 months following failure, the near-dam reservoir reach steepened from a gradient of 0.005 up to 0.012 (Table I). During this period, we see no substantial evidence of channel response at the far-upstream reach (Figures 4(a), (b) and 6(c)), except that the cross-section located 2450 m upstream of the dam incised 1.8 m in the 3 months post-failure, which we approximate as the most upstream evidence of knickpoint migration during the first survey period. These patterns of change in gradients, erosion rates, cross-sections, and the longitudinal profile indicate that the knickpoint migrated approximately 2450 m upstream during the first 3 months and that the channel eroded the stored material primarily through channel-spanning incision.
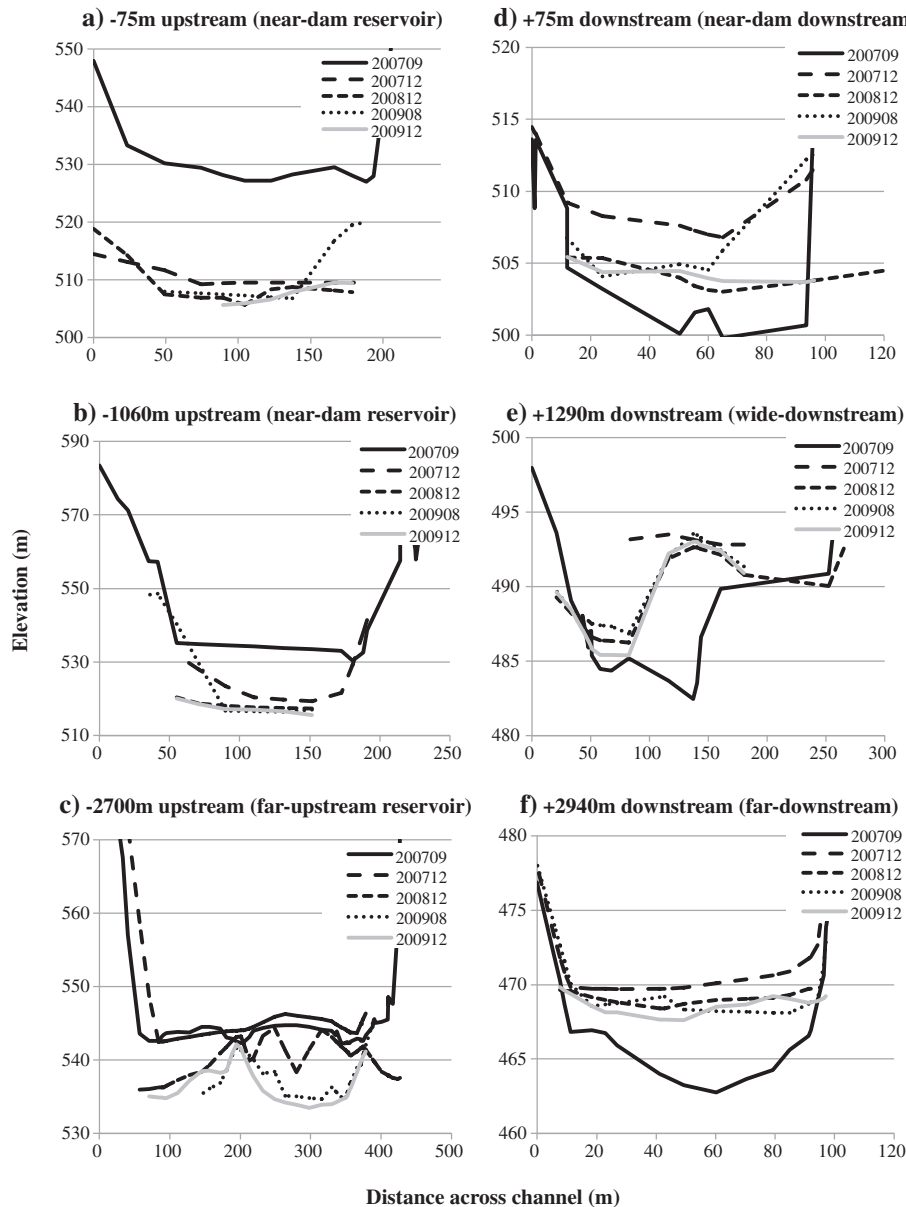
**a) -75m upstream (near-dam reservoir)**

**d) +75m downstream (near-dam downstream)**

**b) -1060m upstream (near-dam reservoir)**

**e) +1290m downstream (wide-downstream)**

**c) -2700m upstream (far-upstream reservoir)**

**f) +2940m downstream (far-downstream)**

**Distance across channel (m)**

**Figure 6.** Representative cross-sectional elevation changes over time. The sub-reaches for each cross-section are indicated in parentheses. Note that the ranges for the x and y axes are not consistent for all the cross-sections.

In subsequent survey periods, the rate of channel incision (Figure 4(a) and (b)) declined in the near-dam reservoir reach and increased in the far-upstream reservoir reach. In contrast to the first time period when there was no discernible change, between December 2007 and December 2008, the highest degree of incision (Figure 4(a)) and maximum rate of change (Figure 4(b)) both occurred in the most upstream cross-section. Channel gradient in this far-upstream reach also steepened between December 2007 and December 2008 while the near-reservoir gradient remained constant (Table I). Beyond December 2008, the far-upstream reach continued to undergo minor (<1 m) incision (Figure 4(a) and (b)) while the elevation of the near-dam reservoir reach remained constant. With one exception (-1060 m), rates of change in cross-sectional area were nearly zero for all reservoir cross-sections by the final survey in December 2009.

Cross-section plots illustrate how the rapid (Figure 6(a) and (b)) and delayed (Figure 6(c)) reservoir responses extended across the channel. Erosion of the near-dam reservoir cross-sections was mostly uniform across the width of the channel. Erosion in the wider, far-upstream reach was not uniform (Figure 6(c)). By December 2008, erosion occurred along both sides of a persistent

but unvegetated mid-channel bar, resulting in a stable configuration of two baseflow channels in the remaining surveys (Figure 4c).

Planform changes also occurred rapidly in the reservoir. For example, the number of channels carrying baseflow at three locations (-75 m, –2450 m, –2700 m) in the reservoir transitioned from two or three channels to a single thread channel by October 2007 (Figure 4(c)). No changes were observed between the 2007 and 2008 aerial photos. However, as discussed above, the plot of the cross-section located 2700 m upstream of the former dam site (Figure 7(c)) indicates that the river transitioned back to two channels following the erosion that occurred during the 2008 typhoon season, which is not represented in the September 2008 aerial photo.

## Rates and patterns of downstream deposition

The timeframes and type of responses were consistent across all downstream reaches, though the degree of change varied by reach. The majority of the channel rapidly aggraded after dam failure (Figures 4(a), (b) and 6(d-f)). By the following survey in December 2008, the channel eroded up to 4 m of the deposited
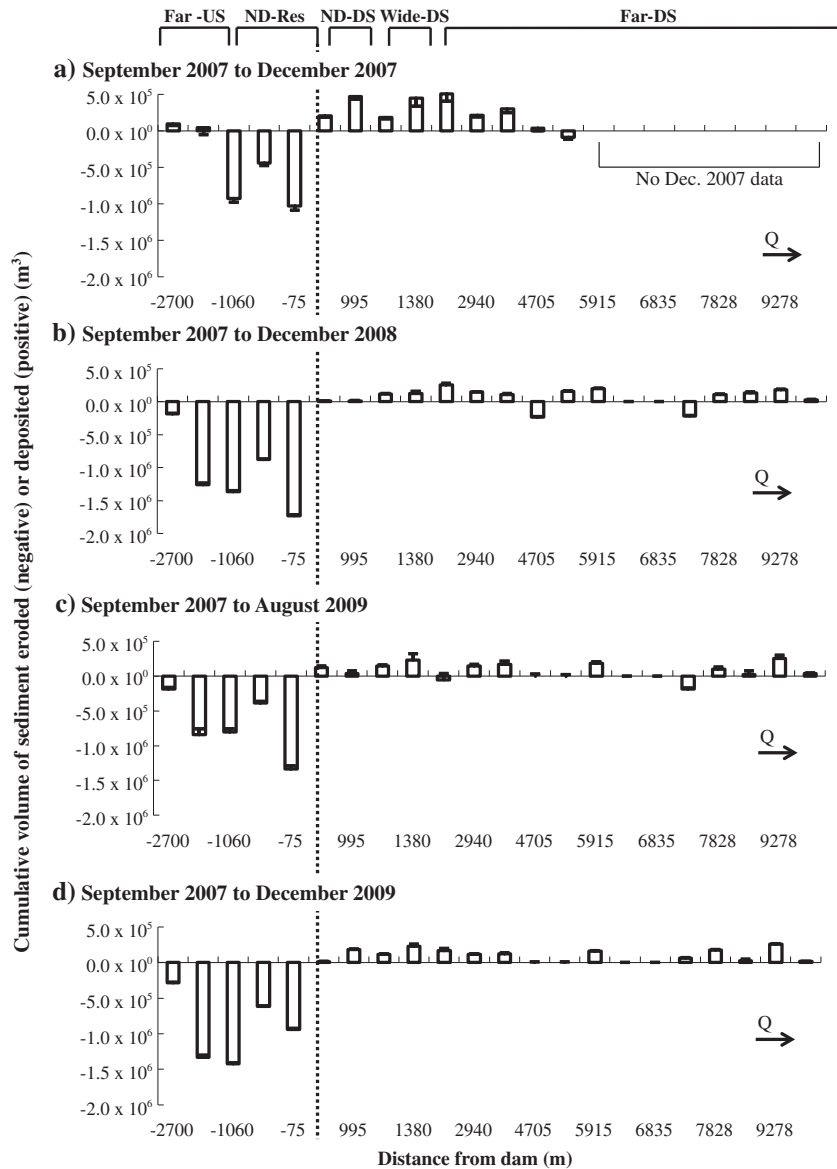
**Figure 7.** Cumulative, net volumes of erosion and deposition, with error estimates. Cumulative estimates are based on differences from the pre-failure surveys. The vertical dashed line represents the location of the dam. Flow (Q) direction is to the right of the page.

material, primarily in the near-dam and wide downstream reaches (Figures 4d and 6(d-e)). Subsequent surveys show little additional change in the thalweg elevation. Only minor (<1 m) incision occurred over subsequent surveys periods (Figure 4(a)) and rates of change in cross-sectional area (Figure 4(b)) were negligible after December 2008. The channel generally remained at an aggraded elevation, with an average of 4 m of deposited material persisting on the bed in the December 2009 survey relative to pre-failure elevations.

However, though the timeframes and types of responses were similar across the downstream study reaches, the amount of deposition varied longitudinally (Figure 4(a)), particularly between the near-dam and wide-downstream reaches. Up to 10 m of aggradation occurred in the wide-downstream reach (Figures 4(a) and 6(e)), while a maximum of only 8.5 m of deposition occurred in the reach immediately below the dam (Figures 4(a) and 6(d)). Of all the downstream cross-sections, the rate of change in cross-sectional area (Figure 4(b)) was greatest in the wide-downstream reach and primarily occurred over the 3 months following dam failure. Beyond the wide-downstream reach, the degree of aggradation in the far downstream reach appears to decrease with increasing distance from the dam.

Other patterns distinguish the responses across the near-dam and wide-downstream study reaches. For example, the gradient in the near-dam downstream reach remained essentially constant across all study periods (Figure 4(a), Table I), reflecting relatively uniform depths of aggradation and subsequent incision along the study reach. In contrast, the wide-downstream reach (Figure 4(a), Table I) channel gradient decreased in the 3 months following dam failure before it stabilized for the duration of the study. The number of channels carrying baseflow over time also distinguishes the downstream reaches. Aerial photos indicate that the number of channels at baseflow did not change in the narrow near-dam reach during any of the study periods (Figure 4(c)). The wide-downstream reach appears to have transitioned from single thread channel in November 2006 to multi-thread channels by October 2007. By the time of the September 2008 aerial photo, the river in the wide-downstream reach transitioned back to single-thread channel 1290 m downstream from the former dam site, and from three to two channels 1380 m downstream (Figure 4(c)).

In the far-downstream reach, evidence of channel responses decreased with distance from the dam site. Up to 7 m of deposition occurred near the top of the study reach (+2940 m) and decreased with distance downstream (Figure 4(a)). The

maximum rate of change in cross-sectional area occurred at the first cross-section within this reach and, like depth of deposition, decreased with distance downstream (Figure 4(b)). Very little variation in the channel gradient was observed across the study periods for the far-downstream reach (Table II). The number of channels at baseflow increased at three cross-sections in the month after failure, then returned to a single-thread channel by September 2008, with no clear relation to distance from the dam site (Figure 4(c)).

## Net volumes of reservoir erosion and downstream deposition across study periods

Cumulative changes in the sediment balance (Figure 7) further illustrate patterns of deposition and erosion. Across all study periods, the magnitude of downstream deposition following dam failure is small relative to the volume eroded from the reservoir (Figure 7). Between September 2007 and December 2007, $4.5 \times 10^6$ m$^3$ more sediment eroded from the reservoir than deposited downstream. The discrepancy between reservoir erosion and downstream deposition is greatest ($6.3 \times 10^6$ m$^3$) during the second study period (Figure 7(b)), when there were the most days of high flows that eroded additional material from the reservoir and transported material through the downstream reach. The erosion-deposition discrepancy then declines to $2.8 \times 10^6$ m$^3$ in the third study period (Figure 7(c)), a period of no high flows, primarily due to deposition within the former reservoir (Figure 6(a-c)). By December 2009, there was $4.8 \times 10^6$ m$^3$ more cumulative erosion detected that deposition (Figure 7(d)), similar to the value estimated three months after failure. These patterns in the sediment balance suggest that much of the sediment eroded from the reservoir was transported beyond the downstream study reach, particularly during Typhoon WeiPa and the high flows in the 15 months that followed.

Reservoir erosion moved from the near-dam reservoir reach to the far-upstream reservoir reach after the first 3 months following dam failure (Figure 7(a)), and changes in the volumes of erosion varied with time and hydrologic conditions. Net erosion occurred primarily in the near-dam reservoir reach over the first 3 months following dam failure (Figure 7(a)), with approximately $2.4 \times 10^6$ m$^3$ of material evacuated within the first 1060 m upstream of the dam. With six days of high flows (Figure 3(b), Table II) occurring between December 2007 and December 2008, erosion extended into the far-upstream reservoir reach, primarily up to the cross-section at −2450 m (Figure 4(a)). By December 2008, additional material was eroded from the near-dam reservoir reach, resulting in net erosion of $5.4 \times 10^6$ m$^3$ for the entire reservoir (Figure 7(b)). However, by August 2009, the net loss of material from the entire reservoir reach (Figure 7(c)) was reduced to $3.5 \times 10^6$ m$^3$. The reduction in eroded volume is associated with approximately $1.8 \times 10^6$ m$^3$ of distributed aggradation that occurred between December 2008 and August 2009, primarily along the margins of the cross-sections in the near-dam reservoir reach (Figure 6(a) and (b)). The typhoon season of 2009, which included two days of high flows (Figure 3(b), Table II), resulted in $4.6 \times 10^6$ m$^3$ net erosion of reservoir sediment by the end of the study period (Figure 7(d)), a value that represents approximately 44% of the reservoir's original storage capacity.

The volume of deposition downstream of the dam also varies by study period, generally reflecting an initial period of deposition followed by erosion of the deposited material. In the near-dam downstream reach, $6.8 \times 10^5$ m$^3$ of sediment deposited within 3 months of failure (Figure 7(a)). This material was subsequently eroded (Figure 7(b)) in the following year, which

experienced six days of high flow (Figure 3(b), Table II). The site-wide deposition that occurred during the period of slack flows between December 2008 and August 2009 is most evident in the near-dam downstream reach (Figures 6(d) and 7(c)) where $1.5 \times 10^5$ m$^3$ of material deposited. Approximately $0.3 \times 10^5$ m$^3$ of the material deposited in the near-dam downstream reach by August 2009 was subsequently eroded by December 2009 (Figure 7(d)).

Temporal patterns of deposited sediment volumes were similar in the wide-downstream reach, with sediment first depositing within 3 months then subsequently eroding in the following year. Approximately $1.1 \times 10^6$ m$^3$ of sediment deposited along the wide-downstream reach in the 3 months following dam failure (Figure 7(a)). Over half of that deposited material eroded from this reach (Figure 7(b)) by December 2008. The channel subsequently eroded an additional $1.8 \times 10^5$ m$^3$ by August 2009 (Figure 7(c)) during the period of slack flows, and then deposited that same volume by December 2009 (Figure 7(d)).

Except locally (+2730 m, +2940 m, +3610 m), the far-downstream reach shows little systematic evidence of a passing sediment pulse (Figure 7). Across the study periods, both deposition (e.g. +5915 m, + 9728 m) and erosion (e.g. +4705 m, +7535 m) occurred locally. However, the deposited volumes are small relative to deposition in the near-dam and wide-downstream reaches in the first post-failure period.

## Hydraulic conditions and sediment transport regimes across study periods

Hydraulic conditions in the downstream reaches, estimated for the peak discharge between study periods, varied substantially, as illustrated by variability in the Shields number, relative submergence of particles (D/d), and grain Reynolds numbers (Table III). The variability in these parameters is associated with differences in the peak flow and size of sediment delivered between surveys, and offers insight regarding variability in dominant sediment processes over time. For example, the Shields number is greater than one in the pre-failure channel (Table III), indicating that the median-sized sediment was mobilized by flows that occurred prior to failure. The high Shields number also suggests that the pre-failure sediment transport processes should be consistent with those observed in labile channels (Dade and Friend, 1998). Generally, the Dahan River does not fit the characteristics of labile channels. Width–depth ratios are mostly greater than 40 (Table III). There are no vegetated islands. The gradient is moderate (s = 0.01). Bed load comprises ~30% of the total load (Dadson et al., 2003). However, consistent with the behavior of labile channels, rates of channel area change following the Barlin Dam failure are rapid relative to other rivers in which a sediment pulse was introduced. For example, the knickpoint migrated approximately 2450 m upstream of the Barlin Dam site within the 3 months (Figure 4 (a)). In comparison, it took 7 months for the knickpoint to migrate 2000 m up the Sandy River following the removal of Marmot Dam (Major et al., 2012). Furthermore, consistent with labile channels, while the substrate is generally gravel-dominated, sand can dominate the substrate of the Dahan River in some years. Thus, both the Shields number and rates of change suggest that sediment processes (e.g. rapid morphological changes, frequent entrainment of sediment, full bed mobility) associated with labile channels may have occurred in the Dahan River prior to dam failure, even though the river generally does not fit many of the labile channel characteristics.

In subsequent study periods, the Dahan River exhibited characteristics of threshold and transitional channels. For example,

**Table III.** Simulated hydraulic and sediment transport characteristics of representative downstream cross-sections at peak flow between survey periods. Parameters are based on results of 1-D HEC-RAS modeling. D = reach averaged D50; d = water depth; $\tau$ = applied shear stress; $\tau_{cr}$ = critical shear stress to mobilize the D50; W = active channel width; DS = downstream. Differences in channel gradients between Table II and Table III are due to averaging across multiple cross-sections in Table II. Gradients reported in Table III for individual cross-sections were calculated as the change in elevation between locations that are half of the distance to adjacent cross-sections

**200709 (Modeled discharge = 92 cms)**

| Study reach | Location | d (m) | Gradient (m/m) | $\tau/\tau_{cr}$ (Nm$^{-2}$/Nm$^{-2}$) | Shields number | D/d (m/m) | W/d (m/m) | Grain Reynolds no. |
|---|---|---|---|---|---|---|---|---|
| near-dam DS | + 75 | 0.8 | 0.016 | 5.0 | 2.5 | 0.007 | 113.9 | 7.70E+03 |
| wide-DS | + 1380 | 1.2 | 0.010 | 3.6 | 2.4 | 0.004 | 214.3 | 6.90E+03 |
| far DS | + 2940 | 0.8 | 0.010 | 5.2 | 1.6 | 0.006 | 124.7 | 7.90E+03 |

**200712 (Modeled discharge = 543 cms)**

| Study reach | Location | d (m) | Gradient (m/m) | $\tau/\tau_{cr}$ (Nm$^{-2}$/Nm$^{-2}$) | Shields number | D/d (m/m) | W/d (m/m) | Grain Reynolds no. |
|---|---|---|---|---|---|---|---|---|
| near-dam DS | + 75 | 1.7 | 0.015 | 8.7 | 0.5 | 0.029 | 50.1 | 1.20E+05 |
| wide-DS | + 1380 | 1.1 | 0.012 | 6.4 | 0.3 | 0.045 | 225.8 | 9.30E+04 |
| far-DS | + 2940 | 1.6 | 0.009 | 8.3 | 0.3 | 0.031 | 62.3 | 1.10E+05 |

**200812 (Modeled discharge = 1716 cms)**

| Study reach | Location | d (m) | Gradient (m/m) | $\tau/\tau_{cr}$ (Nm$^{-2}$/Nm$^{-2}$) | Shields number | D/d (m/m) | W/d (m/m) | Grain Reynolds no. |
|---|---|---|---|---|---|---|---|---|
| near-dam DS | + 75 | 2.9 | 0.015 | 12.5 | 0.8 | 0.017 | 29.6 | 1.50E+05 |
| wide-DS | + 1380 | 2.7 | 0.011 | 11.0 | 0.6 | 0.020 | 101.6 | 1.40E+05 |
| far-DS | + 2940 | 3.5 | 0.008 | 14.0 | 0.6 | 0.014 | 29.1 | 1.60E+05 |

**200908 (Modeled discharge = 27 cms)**

| Study reach | Location | d (m) | Gradient (m/m) | $\tau/\tau_{cr}$ (Nm$^{-2}$/Nm$^{-2}$) | Shields number | D/d (m/m) | W/d (m/m) | Grain Reynolds no. |
|---|---|---|---|---|---|---|---|---|
| near-dam DS | + 75 | 0.4 | 0.017 | 3.1 | 0.1 | 0.143 | 247.4 | 5.30E+04 |
| wide-DS | + 1380 | 0.7 | 0.010 | 2.0 | 0.2 | 0.068 | 346.4 | 4.80E+04 |
| far-DS | + 2940 | 0.3 | 0.007 | 3.0 | 0.1 | 0.147 | 297.1 | 5.20E+04 |

**200912 (Modeled discharge = 442 cms)**

| Study reach | Location | d (m) | Gradient (m/m) | $\tau/\tau_{cr}$ (Nm$^{-2}$/Nm$^{-2}$) | Shields number | D/d (m/m) | W/d (m/m) | Grain Reynolds no. |
|---|---|---|---|---|---|---|---|---|
| near-dam DS | + 75 | 1.4 | 0.017 | 7.5 | 0.5 | 0.004 | 61.4 | 1.00E+05 |
| wide-DS | + 1380 | 1.9 | 0.010 | 7.0 | 0.4 | 0.003 | 131 | 1.10E+05 |
| far-DS | + 2940 | 1.4 | 0.007 | 7.4 | 0.2 | 0.004 | 74.3 | 1.00E+05 |

in the study periods that followed the typhoon seasons (December 2007, December 2008, December 2009), high flow conditions associated with typhoons resulted in Shields numbers within the range of transitional channels. Between December 2008 and August 2009, flows never reached the 1.5RYI (Table II, Figure 3(c)), and bed material remained coarser than pre-failure substrates. As a result, Shields numbers dropped below 0.15 (Table III), suggesting conditions associated with threshold channels. Alternately, higher flows resulted in higher Shields numbers in the range 0.3 to 0.8 for September 2007 to December 2008, conditions more representative of transitional transport regimes.

This emergence of threshold and transitional channels suggests that different sediment transport processes dominated across the study periods. For example, transport in threshold channels is typically bed load dominated whereas transitional channels carry mixed loads, with a large proportion moving in suspension. Rates of morphological changes in average water years are typically higher in transitional than in threshold channels. Bed mobility in threshold channels is characterized by partial and size-selective transport, with full mobility only in exceptionally large events, whereas full mobility occurs more frequently in transitional channels. Deposition generates low, alternating bars in threshold channels, while deposition in transitional channels can result in general aggradation of the bed, generating lateral instability and scour (Church, 2006). These differences in sediment transport processes that likely occurred in the Dahan River across the study periods, driven by basin-scale sediment and water delivery to the study site, may be related to the observed rates of change in channel gradient (Figure 4(a)), cross-section area (Figures 4(b) and 6), and volumes of scour and deposition (Figure 7).

The pattern of varying sediment transport processes across study periods is further demonstrated by comparing hydraulic parameters (Table III), estimated for observed peak flows, to

established relations between grain Reynolds number and Shields number (Figure 8(a)), and between relative roughness (D/d) and channel gradient (Figure 8(b)). The pre-failure channel plots in the region of mixed-load transport region of the Shields diagram (Figure 8(a)) and in the region of suspended-load transport on the gradient-roughness relation (Figure 8(b)). These results support the finding that sediment processes associated with labile channels, including suspension-dominated transport, likely prevailed prior to dam failure. In contrast, hydraulic and sediment conditions for all 12 of the post-failure cross-sections plot within the mixed load region of both relations (Figure 6). With mixed load dominating sediment transport, the threshold and transitional channel is expected to be more stable than the labile channel, experiencing lower transport rates and only partial transport of bed material. These results highlight how the peak flows and size of sediment supplied to the channel relate to sediment processes across the site. The hydraulic and sediment conditions likely intensified the rapid rate of channel change immediately following failure and contributed to the decrease in rates of change for subsequent survey periods.

## Discussion

### Channel morphology

Patterns of reservoir erosion generally varied with distance from the dam, valley width, and temporal variability in basin-scale hydrology and sediment inputs across the study periods. The role of distance from the dam and valley width in regulating channel response is evident in the timing of reservoir erosion. For example, the reservoir underwent rapid knickpoint migration in the narrow, near-dam reservoir reach, while incision was delayed up to 15 months in a wider reach farther upstream.
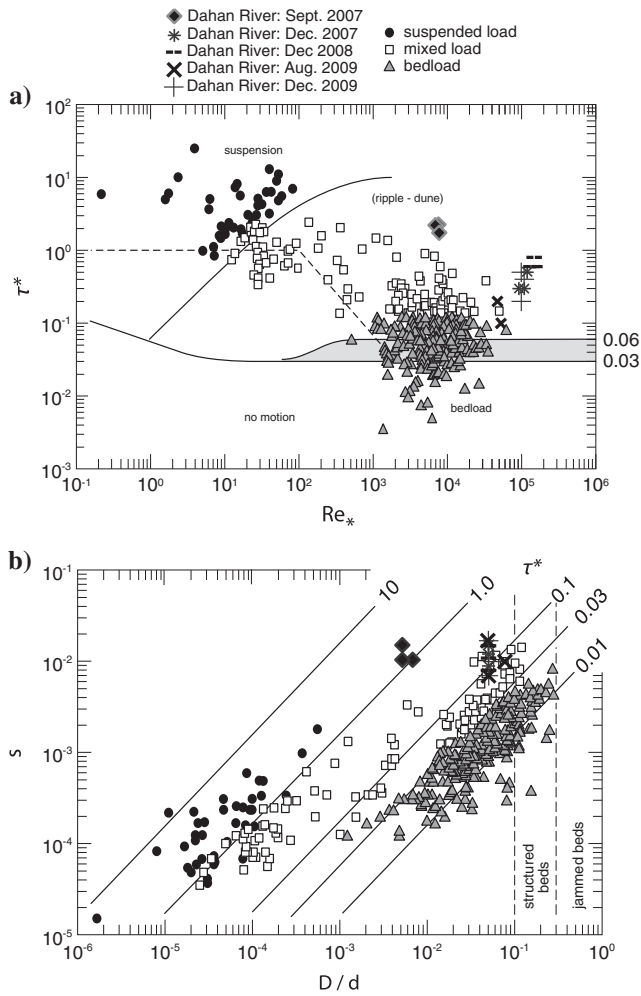
**Figure 8.** Simulated hydraulic and sediment conditions at peak flows between study periods relative to published studies and sediment transport regimes. Approximate boundaries between sediment regimes are superimposed on plots of (a) Shields diagram, with the grain Reynolds number plotted against the Shields number, and (b) gradient vs. relative roughness (D/d), where D = median (D50) grain size for the study period and d = water depth at peak flow between the survey periods. Straight lines in Figure 8(b) represent constant $\tau^*$. Figures are adapted from Church (2006), with permission, and include data from Dade and Friend (1998).

The importance of exogenous variability in the hydrologic and sediment regimes is illustrated by the orders of magnitude coarsening in bed material that occurred study-wide by November 2008 (Figure 5) and by the deposition in the reservoir during the December 2008 to August 2009 period of slack flows (Figure 7).

No evidence of channel widening was observed in the reservoir cross-sections (Figure 6) or aerial photos. Instead, the channel gradient rapidly adjusted then stabilized, within 3–15 months depending on the reach (Figure 4(a), Table I). This result does not document the common erosional sequence of incision followed by widening (Doyle *et al.*, 2003; Cantelli *et al.*, 2007). The lack of observed widening is likely associated with the resistant bedrock lining the valley walls (Figure 4(a)) and a lack of substantial floodplain in this section of the Dahan River that would limit extensive lateral adjustments. However, it is also possible that the channel incised and then widened nearly simultaneously, as has been observed elsewhere (Major *et al.*, 2012) over the 3 months between the dam failure and the first post-failure survey.

In the downstream reaches, patterns of deposition also varied with distance from the dam, valley width, and study period. Channel-wide aggradation (Figures 4, 6 and 7) occurred primarily in the 3600 m below the former dam site. Depths (Figure 4(a)) and volumes (Figure 7) of deposited sediment and rates of change in cross-sectional areas (Figure 4(b)) generally decreased with distance from the dam. However, illustrating the effect of valley configuration, rates and magnitudes of change were highest in the wide-downstream reach, a result of the higher transport capacity in the near-dam downstream reach. Finally, the role of exogenous hydrology and sediment regimes are evident from the observation of additional deposition in the August 2009 study period (Figures 6(d) and 7), after it appears the sediment pulse had passed through the downstream reach. The evidence of the passing sediment pulse is based on the sediment budget. The greatest volume (Figure 7(a)) and depths (Figures 4(a) and 6) of aggradation primarily occurred in the 3 months after the dam failure. In the following 12 months, over half of the deposited material was eroded (Figure 7(b)). It is after this sequence of deposition and erosion that additional deposition was observed during the slack flows (Table II, Figure 3(c)) of September 2009. This deposition, which occurred across the entire study reach illustrates of the control basin-scale hydrology exerts on channel response to a sediment pulse.

## Sediment processes and channel responses

On the Dahan River, the variability in sediment and water delivered to the channel across the study periods appear to influence the sediment processes and channel morphology. However, valley configuration also appears to plays a dominant role in driving channel morphology, possibly obscuring the effect of varying sediment transport regimes. As predicted by common channel morphology classifications (Schumm, 1963; Church, 2006), our results indicate that the dominant sediment transport processes varies with the discharge and the quantity and size of sediment delivered to the channel across the study periods. These basin-scale transport processes appear to exert a strong control on the locally-observed rates and types of channel adjustments following the failure of Barlin Dam. For example, the pre-failure substrate across the study area, including sediment reference sites far upstream of the reservoir, was predominantly sand, whereas the substrate post-failure was dominated by gravel and cobble. It is likely that the finer grain size distribution observed at all of the sites before dam failure is due to the burying of the coarser substrate with landslide material. In 2004, Taiwan experienced one of its largest typhoons (Aere) in history. This typhoon triggered a large number of landslides throughout the Dahan River basin (TWRA, 2009; Ho *et al.*, 2012) in 2005 and 2006, which contributed fine material to the river (Wang, 2012). This accumulation of fine material primed the channel for rapid channel change when the dam failed. At least initially, sediment transport processes were most likely those associated with labile channels, with a fully mobile bed, unstable planform, and suspension-dominated transport. Consistent with labile channel morphologies, rates of channel change were rapid, and some evidence of braiding was observed in aerial photos at the widest locations of the downstream reach immediately following dam failure.

Between December 2008 and August 2009, deposition occurred in both the reservoir and downstream reaches. The shallower depths associated with this deposition, in combination with slack flows over this study period and the coarsening that had occurred in the previous year, contribute to river

behavior more consistent with a threshold channel. During this period, sediment would have been transported bed load, with partial to full mobility, though it does not appear that adequate floods occurred to mobilize the sediment. Instead, deposition occurred across the entire study reach. This result highlights how the dominance of sediment transport processes was likely governed more by basin-wide sediment and discharge regimes than by changes in gradient associated with the dam failure over this study period.

It is also clear that major features of the channel morphology at this site are likely governed as much by the valley-forced meandering and resistant valley wall material as they are by the dominant sediment transport regime. For example, as the reservoir incised and the downstream channel aggraded, locations of bars and channel widths remained roughly the same, controlled by valley meandering. This valley-control on channel responses likely explains why some of the common associations between the sediment transport regimes and mor-phological features, including planform, bedform, geometry, and lateral instability, are not widely observed in our results. However, we also note that the survey data are not adequate for distinguishing threshold and transitional channels on the basis of bed structure, or for documenting the presence or movement of sandy bedforms common in labile channels.

## Conclusions

In alluvial rivers, channel morphology is defined by the size and quantity of sediment delivered to it (Church, 2006), and channels generally adjust their pattern, geometry, slope, and roughness in response to changes in sediment supply (Madej, 2001). However, the rates and types of channel adjustments vary along a river basin with hydrologic, topographic, and sed-iment characteristics of the landscape and within an individual river reach based on local variability in transport capacity (Lisle et al., 2000). Field studies can be important for identifying the timescales and likely range of channel responses when they lead to results that can link sediment transport processes and channel morphology (Nanson and Knighton, 1996).

In this paper, we report results on a field-based study of the rates and types of channel adjustments, and the likely sediment transport conditions, that occurred following the failure of Barlin Dam. This study was conducted in an area of the world with strongly seasonal hydrology, high discharge and sediment yields, moderate to steep gradients, and event-driven (e.g. typhoons, earthquakes, landslides) sediment delivery and transport (Milliman and Kao, 2005). The study reach is a moderate gradient, fourth-order river, where bar topography develops under local flow convergence and divergence forced by valley meandering (Lisle, 1986; Montgomery and Buffington, 1997).

Our results indicate that rates of channel change appear to be driven as much by basin-wide hydrologic and sediment conditions and valley configuration as by distance from the dam, as has been observed (Kasai et al., 2004) in other areas subject to remarkably high flows and sediment loads. Channel response to the failure of Barlin Dam was rapid and generally decreased with time and distance from the dam. However, channel adjustments varied substantially across the study periods with variability in sediment and discharge regimes and across the study reaches with variability in channel width and gradient. The dominant mode of sediment transport appears to vary within and between years, with labile channel conditions contributing to more rapid channel change than threshold and transitional channels. Differences in valley width that define local variation in transport capacity also result in

variation in the magnitudes and timing of erosion and deposition. Broadly, the identification of dominant sediment transport regime in the Dahan River offers basin-scale insight regarding the rates and nature of morphological adjustments associated with sediment pulses. The results illustrate how information regarding valley configuration, seasonal variability in discharge, and the amount and caliber of episodic inputs of sediment are all needed to explain where, when, and why sediment pulses are stored and mobilized.

## References

Bartley R, Rutherfurd I. 2005. Measuring the reach-scale geomorphic diversity of streams: Application to a stream disturbed by a sediment slug. *River Research and Applications* **21**: 39–59.

Cantelli A, Wong M, Parker G, Paola C. 2007. Numerical model linking bed and bank evolution of incisional channel created by dam re-moval. *Water Resources Research* **43**: 1–16.

Church M. 2006. Bed Material Transport and the morphology of allu-vial river channels. *Annual Review of Earth and Planetary Sciences* **34**: 325–354.

Dade WB, Friend PF. 1998. Grain-size, sediment transport regime, and channel slope in alluvial rivers. *Journal of Geology* **106**: 661–675.

Dadson SJ, Hovius N, Chen H, Dade WB, Hsieh ML, Willett SD, Hu JC, Horng MJ, Chen MC, Stark CP, Lague D, Lin JC. 2003. Links between erosion, runoff variability and seismicity in the Taiwan orogen. *Na-ture* **426**: 648–651.

Doyle MW, Stanley EH, Harbor JM. 2002. Geomorphic Analogies for Assessing Probable Channel Response to Dam Removal. *Journal of the American Water Resources Association* **38**(6): 1567–1579.

Doyle MW, Stanley EH, Harbor JM. 2003. Channel adjustments following two dam removals in Wisconsin. *Water Resources Research* **39**(1): 1-15.

Fuller IC, Large ARC, Charlton ME, Heritage GL, Milan DJ. 2003. Reach-scale sediment transfers: An evaluation of two morphological budgeting approaches. *Earth Surface Processes and Landforms* **28**(8): 889–903.

Gran KG, Montgomery DR. 2005. Spatial and temporal patterns in fluvial recovery following volcanic eruptions: Channel response to basin-wide sediment loading at Mount Pinatubo, Philippines. *GSA Bulletin* **117**(1/2): 195–211.

Hassan MA, Zimmermann AE. 2012. Channel response and recovery to changes in sediment supply. In Gravel-Bed Rivers: Processes, Tools, Environments, Church M, Biron P, Roy A (eds). John Wiley and Sons: Chichester UK; 464–473.

Ho HC, Lin BS, Chi SY, Chung CR, Chiu SY. 2012. Spatio-temporal Analysis for Landslide change and Remediation Efficiency in Shih-Men Reservoir Watershed. *Journal of Soil and Water Technology* **7**(3): 174–188

Hoffman D, Gabet E. 2007. Effects of sediment pulses on channel morphology in a gravel-bed river. *GSA Bulletin* **119**(1-2): 116–125.

Humphries R, Venditti JG, Sklar LS, Wooster JK. 2012. Experimental evidence for the effect of hydrographs on sediment pulse dynamics in gravel-bedded rivers. *Water Resources Research* **48**: 1–15. DOI: 10.1029/2011WR010419

Kasai M, Marutani T, Brierley G. 2004. Patterns of sediment slug translation and dispersion following typhoon-induced disturbance, Oyabu Creek, Kyushu, Japan. *Earth Surface Processes and Landforms* **29**: 59–76.

Leopold LB, Wolman MG, Miller JP. 1964. Fluvial Processes in Geomorphology. Freeman: San Francisco.

Lisle TE. 1986. Stabilization of a gravel channel by large streamside obstructions and bedrock bends, Jacoby Creek, northwestern California. *Geological Society of America Bulletin* **97**: 999–1011.

Lisle TE. 2008. The evolution of sediment waves influenced by varying transport capacity in heterogeneous rivers. In Gravel-bed Rivers VI: From Process Understanding to River Restoration, Habersack H, Piegay H, Rinaldi M (eds). Elsevier: Amsterdam, The Netherlands; 213–239. DOI: 10.1016/S0928-2025(07)11136-6

Lisle TE, Nelson J, Pitlick J, Madej MA, Barkett BL. 2000. Variability of bed mobility in natural, gravel-bed channels and adjustments to sediment load at local and reach scales, *Water Resources Research* **36**(12): 3743–3755.

Lisle TE, Cui Y, Parker G, Pizzuto JE, Dodd AM. 2001. The dominance of dispersion in the evolution of bed material waves in gravel-bed rivers. *Earth Surface Processes and Landforms* **26**: 1409–1420.

Madej MA. 2001. Development of channel organization and roughness following sediment pulses in single-thread, gravel bed rivers. *Water Resources Research* **37**: 2259–2272.

Madej MA, Ozaki V. 1996. Channel response to sediment wave propagation and movement, Redwood Creek, California, USA. *Earth Surface Processes and Landforms* **21**: 911–927.

Major JJ, O'Connor JE, Podolak CJ, Keith MK, Grant GE, Spicer KR, Pittman S, Bragg HM, Wallick JR, Tanner DQ, Rhode A, Wilcock PR. 2012. Geomorphic response of the Sandy River, Oregon, to removal of Marmot Dam. USGS Professional Paper 1792.

Milliman JD, Kao SJ. 2005. Hyperpycnal discharge of fluvial sediment to the ocean: Impact of Super-Typhoon Herb (1996) on Taiwanese Rivers. *Journal of Geology* **113**: 503–506

Milan DJ, Heritage GL, Hetherington D. 2007. Application of a 3D laser scanner in the assessment of erosion and deposition volumes and channel changes in a proglacial river. *Earth Surface Processes and Landforms* **32**(11): 1657–1674.

Montgomery DR, Buffington JM. 1997. Channel-reach morphology in mountain drainage basins. *Geological Society of America Bulletin* **109**: 596–611.

Nanson GC, Knighton AD. 1996. Anabranching rivers: their cause, character and classification. *Earth Surface Processes and Landforms* **21**: 217–239.

Pizzuto J. 2002. Effects of dam removal on river form and process. *BioScience* **52**(8): 683–691.

Sawaske SR, Freyberg DL. 2012. A comparison of past small dam removals in highly sediment-impacted systems in the U.S. *Geomorphology* **151–152**: 50–58.

Schumm SA. 1963. A tentative classification of alluvial river channels. Circular 477, U.S. Geological Survey: Washington, DC.

Simon A, Curini A, Darby SE, Langendoen EJ. 2000. Bank and near-bank processes in an incised channel. *Geomorphology* **35**: 193–217.

Sklar LS, Fadde J, Venditti J, Nelson P, Wydzga MA, Cui Y, Dietrich WE. 2009. Translation and dispersion of sediment pulses in flume experiments simulating gravel augmentation below dams. *Water Resources Research* **45**: 1–14. DOI: 10.1029/2008WR007346.

Taiwan Water Resources Agency. 2006. Evaluation Study of Landslide Susceptibility and Landslide Size in Reservoir Watersheds (in Chinese).

Taiwan Water Resources Agency. 2007. Preliminary Investigation of Barlin Dam Failure (in Chinese).

Taiwan Water Resources Agency. 2009. Evaluation for effectiveness of sediment reduction conservation engineering in Shihmen Reservoir Catchment Area (in Chinese).

USACE. 2011. HEC-RAS version 4.1. Available online at: http://www.hec.usace.army.mil/software/hec-ras/index.html

Venditti JG, Dietrich WE, Nelson PA, Wydzga MA, Fadde J, Sklar LS. 2010. Effect of sediment pulse grain size on sediment trans- port rates and bed mobility in gravel bed rivers. *Journal of Geophysical Research* **115**: 1–19. DOI: 10.1029/2009JF001418.

Walter C, Tullos D. 2010. Downstream channel changes after a small dam removal: Using aerial photos and measurement error for context; Calapooia River, Oregon. *River Research and Applications* **28**: 1220–1245. DOI: 10.1002/rra.1323

Wang HL. 2012. Research on Riverbed Variation in Shoufeng River. Master Thesis, National Cheng Kung University (in Chinese)

Williams GP. 1978. Bank-full discharge of rivers. *Water Resources Research* **14**(6): 1141–1153.

Wheaton JM, Brasington J, Darby SE, Sear DA. 2010. Accounting for uncertainty in DEMs from repeat topographic surveys: Improved sediment budgets. *Earth Surface Processes and Landforms* **35**: 136–156.

Wohl EE, Cenderelli DA. 2000. Sediment deposition and transport patterns following a reservoir sediment release. *Water Resources Research* **36**: 319–333.

Wolman MG, Gerson R. 1978. Relative scales of time and effectiveness of climate in watershed geomorphology. *Earth Surface Processes* **3**: 189–208.